PCCP

View Online
Dynamic Article Links

Cite this: DOI: 10.1039/c0cp02477e

www.rsc.org/pccp

PAPER

Sandwich-type functionalized graphene sheet-sulfur nanocomposite for rechargeable lithium batteries†‡

Yuliang Cao,[ab] Xiaolin Li,[a] Ilhan A. Aksay,[c] John Lemmon,[a] Zimin Nie,[a] Zhenguo Yang[a] and Jun Liu*[a]

Received 10th November 2010, Accepted 8th March 2011
DOI: 10.1039/c0cp02477e

A functionalized graphene sheet-sulfur (FGSS) nanocomposite was synthesized as the cathode material for lithium–sulfur batteries. The structure has a layer of functionalized graphene sheets/stacks (FGS) and a layer of sulfur nanoparticles creating a three-dimensional sandwich-type architecture. This unique FGSS nanoscale layered composite has a high loading (70 wt%) of active material (S), a high tap density of $\sim$0.92 g cm^{-3}, and a reversible capacity of $\sim$505 mAh g^{-1} ($\sim$464 mAh cm^{-3}) at a current density of 1680 mA g^{-1} (1C). When coated with a thin layer of cation exchange Nafion film, the migration of dissolved polysulfide anions from the FGSS nanocomposite was effectively reduced, leading to a good cycling stability of 75% capacity retention over 100 cycles. This sandwich-structured composite conceptually provides a new strategy for designing electrodes in energy storage applications.

Introduction

Lithium–sulfur batteries have been studied as one of the most promising systems for the next generation high-energy rechargeable lithium batteries because of their high theoretical specific capacity ($\sim$1680 mAh g^{-1}) and energy density (2600 Wh kg^{-1}).[1–3] However, the poor electrical conductivity of elemental sulfur and the fast-capacity degradation from polysulfide dissolution into the electrolyte have greatly limited its practical applications.[4–7] Over the past several decades, extensive research has been carried out to address these problems.[8–25] Conductive polymers and carbon networks have been widely investigated to improve the conductivity of the composites containing sulfur.[8–14] Polymer modification,[9,16–17] alternative electrolytes,[18–21] and electrolyte additives[22–23] have been tested to mitigate the problem of polysulfides dissolving in electrolytes.[4,8,15] Recently, important progress was made by using sulfur and mesoporous carbon nanocomposites as the cathode for Li–S batteries.[9] A high reversible capacity of 1320 mAh g^{-1} and an 83% capacity retention over 20 cycles were achieved at a 0.1C discharge rate (168 mA g^{-1}).[9] Progress was also made on sulfur-based batteries using a polymer/tin composite or silicon as anode materials.[24–25]

In this study, we synthesized a functionalized graphene sheets-sulfur nanocomposite (FGSS), a sandwich-type architecture containing functionalized graphene sheets/stacks (FGSs)[26,27] and a layer of sulfur nanoparticles. Furthermore, we here demonstrate the application of these nanoscale sandwich-structures as the cathode material for lithium–sulfur batteries. Graphene, with its excellent conductivity (electron mobility 200 000 cm^2 V^{-1} s^{-1}) and a large surface area (2630 m^2 g^{-1}, calculated value),[28,29] has been widely studied in electrochemical energy storage devices, such as lithium ion batteries, to improve the conductivity and stability of the composite electrode.[30–33] Additionally, graphene is also a useful nanoscale building block for producing composite materials with polymer or metal oxide nanoparticles.[30–35] Very recently, sulfur was mixed with graphene that was prepared by solvothermal synthesis. The material indeed showed a higher conductivity and better capacity retention than pure sulfur.[36] However, the sulfur loading was extremely low (17 to 22 wt%) and the capacity decreased from $>$1100 mAh/g to $\sim$600 mAh/g at 0.03C within 40 cycles. Therefore, other methods to achieve higher sulfur loading and to protect the polysulfide from dissolution need to be developed.

The FGSs for this work were prepared by a thermal expansion of graphite oxide that contains approximately 80 wt% single sheet graphene along with stacked graphene (graphene stacks). The carbon to oxygen ratio of the graphene material is about 14, which allows the FGSs to retain a good electrical conductivity.[26,27]

The new sandwich-type structure allows a much higher sulfur loading and more uniform distribution of the sulfur nanoparticles in carbon, resulting in a much higher reversible capacity at fast charge/discharge rates. Further improvement

[a] *Pacific Northwest National Laboratory, Richland, WA 99352, USA. E-mail: Jun.Liu@pnl.gov*
[b] *Department of Chemistry, Wuhan University, Wuhan 430072, P. R. China*
[c] *Department of Chemical and Biological Engineering, Princeton University, Princeton, NJ 08544, USA*

† Electronic supplementary information (ESI) available. See DOI: 10.1039/c0cp02477e

‡ This article was submitted following the 1st workshop on Energy Materials, organised by The Thomas Young Centre, and held on 7–9 September 2010 at University College London.

in capacity retention can be accomplished by addition of a polymer coating. After coating with Nafion®, this FGSS composite, when tested as the cathode in lithium–sulfur batteries, has a high reversible capacity of ~960 mAh g^{-1} at 0.1C with a good cycling stability evidenced by >70% capacity retention over 100 cycles. Even at 1680 mA g^{-1} (1C), a large reversible capacity of ~505 mAh g^{-1} is retained over more than 100 cycles.

Experimental

Synthesis of FGSS nanocomposites

Sulfur was first dissolved in carbon disulfide (CS_2) to form a 10 wt% solution. Functionalized graphene (~80 mg, Vor-x from Vorbeck Materials Corporation, Jessup, MD) was added to 3.2 g of the 10 wt% sulfur-CS_2 solution. The mixture was then sonicated with a Branson Sonifier S-450A for 15 min to obtain a homogeneous solution. Subsequently CS_2 was allowed to completely evaporate from the reaction mixture while stirring. The obtained powder was heated at 155 °C under nitrogen gas; a treatment that lowers the viscosity of the sulfur and thereby increases the sulfur loading and distribution on the surface of graphene through capillary action. The sample was then ground with high-energy ball milling (8000 M Mixer/Mill, SPEX, USA) for 8 h to improve the mixing of graphene and sulfur.

Synthesis of Nafion®-coated FGSS Nanocomposites

Commercially available Nafion solution (20 wt% Nafion solution; Sigma-Aldrich) was diluted with deionized water to

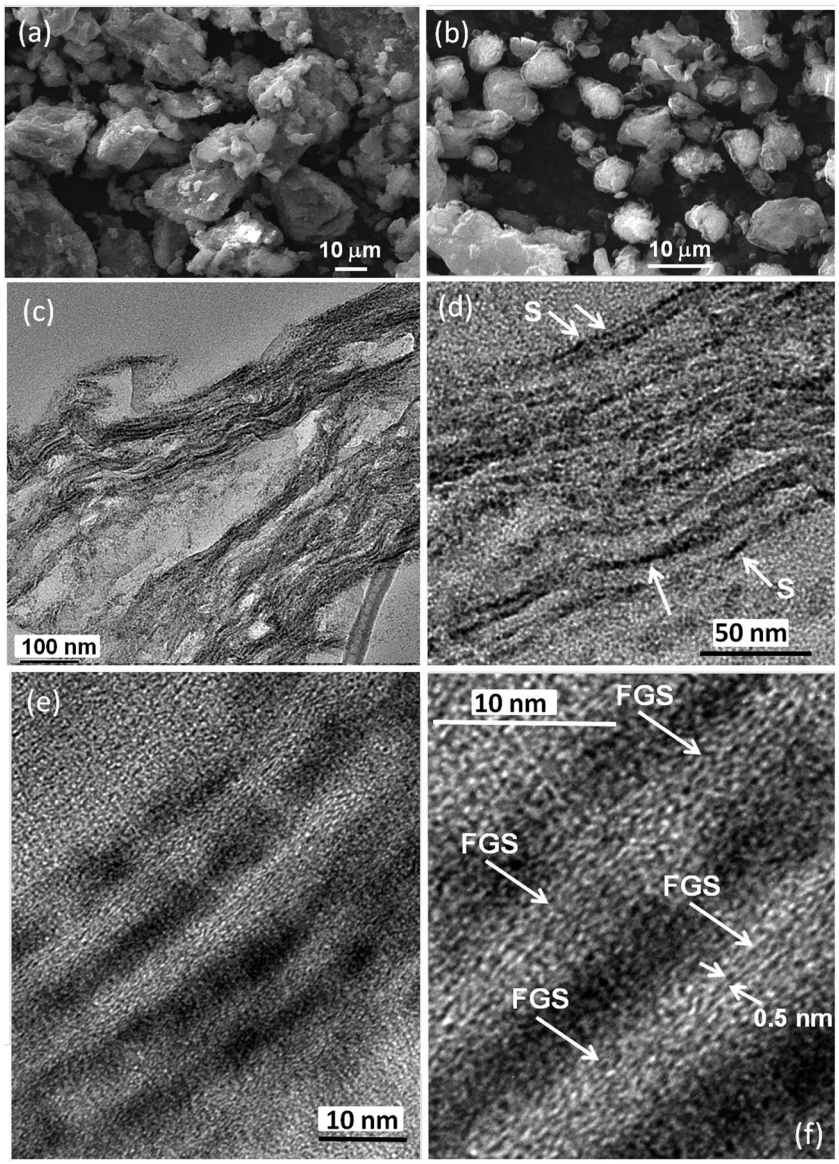

Fig. 1 (a) SEM image of the uncoated FGSS nanocomposite. (b) SEM image of the Nafion-coated FGSS nanocomposite. (c) and (d) Cross-sectional TEM images of the Nafion-coated FGSS nanocomposite depicting the layered sandwich-type architecture of the material. (e) HRTEM image of the Nafion-coated FGSS nanocomposite, dark areas represent sulfur nanoparticles. (f) Magnified HRTEM image of the Nafion-coated FGSS nanocomposite.

a 0.1 wt% solution (~0.5 g Nafion) and mixed with the FGSS nanocomposite (~100 mg). The mixture was continuously stirred for 12 h and then dried by heating to 80 °C under stirring and subsequent vacuum drying.

Structure characterization

Scanning electron microscopy (SEM) and transmission electron microscopy (TEM) experiments were performed on a FEI Helios Nanolab dual-beam focused ion beam/scanning electron microscope (FIB/SEM) and a JEOL-2010 high-resolution transmission electron microscope, respectively. For the TEM study, the Nafion-coated FGSS nanocomposite sample was embedded in resin (LR White Resin, Electron Microscopy Sciences) and aged at 60 °C for 20 h. The specimen was then cross-sectioned using an ultramicrotome. Powder X-ray diffraction (XRD) characterization was carried out on a Philips Xpert X-ray diffractometer using Cu Kα radiation at $\lambda = 1.54$ Å. Thermal gravimetric analysis (TGA) and differential scanning calorimetry (DSC) were conducted with a TGA/DSC 1 (Mettler Toledo) thermogravimetric analyzer in argon at a scan rate of 10 °C/min from room temperature to 800 °C. The Brunauer-Emmett-Teller (BET) surface area was determined through nitrogen adsorption isotherms using a Quantachrome autosorb automated gas sorption system. For conductivity measurements performed using a Modulab system (Solartron Analytical), tested specimens were pressed into pellets at 670 MPa using Midvale-Heppenstall pressure equipment and a 6.5 mm KBr pellet die.

Electrochemical test

The cathode was prepared by mixing 80 wt% FGSS nanocomposite, 10 wt% sp-type carbon black (TIMCAL, Graphite & Carbon Ltd), and 10 wt% polyvinylidene difluoride (PVDF; Alfa Aesar) dissolved in *N*-methyl-2-pyrrolidone (NMP; Aldrich) to form a slurry, which was then pasted as the electrode on an Al foil. Electrochemical tests of the electrode materials were performed using coin cells with the FGSS cathode and lithium metal as the counter and reference electrode. The electrolyte was 1 M bis(trifluoromethane)-sulfonamide lithium salt (LiTFSI; 99.95% trace metals basis; Aldrich) dissolved in a mixture of 1,3-dioxolane (DOL) and dimethoxymethane (DME) (1 : 1 by volume). A microporous membrane (Celgard 2400) was used as the separator. The cells were assembled in an argon-filled glove box. The galvanostatic charge–discharge test was conducted at a voltage interval of 1.0–3.0 V using a BT-2043 Arbin Battery Testing System. Cyclic voltammetry measurements were also carried out with the coin cell at a scan rate of 0.1 mV s^{-1} by using a SI 1287 electrochemical interface (Solartron).

Results and discussion

The observed macroscopic morphologies of the FGSS composite before (Fig. 1a) and after (Fig. 1b) Nafion coating as revealed by SEM studies are very similar. The slightly smaller particle size of the Nafion-coated FGSS composite material is most likely due to additional stirring and resulting breakage during the coating process. Cross-sectional TEM images (Fig. 1c–f) reveal the lamellar structure of the sample to which we have referred as sandwich-type architecture throughout this publication. Over the length scale of several hundred nanometers dark lines interfaced with brighter ones are distinguishable (Fig. 1c). At higher magnification (Fig. 1d and e) it becomes apparent that the darker lines are composed of connected individual nanoparticles. The identity of the S nanoparticles is confirmed by energy dispersive spectroscopy (EDS). HRTEM (Fig. 1f) also shows the alternating graphene sheets/stacks (light contrast) intercalated with layers of sulfur nanoparticles (dark areas). Each sulfur nanoparticle layer is ~5 nm thick and enclosed on both sides by 3–6 nm thick graphene stacks (Fig. 1f). This observation of a layered architecture for our FGSS composite material is in agreement with previous work on SnO_2–graphene, TiO_2–graphene and SiO_2–graphene composite materials.[31,37]

In Fig. 1f the (0002) planar spacing of the undulated graphene stacks is visible. The lattice fringes are ~4.3–5.5 Å apart, which is larger than the 3.4 Å, (0002) planar spacing of graphite but smaller than that of fully oxidized graphite oxide (7.1 Å), and in agreement with a C/O ratio of ~14 for the functionalized graphene sheets/stacks.[26,27] The selected area electron diffraction (SAED) pattern recorded along (Fig. S1a†) the [0001] zone axis reveals the typical six fold symmetric diffuse spots. The SAED pattern perpendicular to the [0001] axis shows two symmetric diffuse spots with elongated shape corresponding to the layer spacing within the graphene stacks (Fig. S1b†).

As discussed, the initial FGSs used in this study contain more than 80 wt% dispersed graphene sheets. In our synthesis, no dispersing agents are used to keep the graphene sheets dispersed as comparing with our previous solution based synthesis approach.[30,31] It is likely that some degree of restacking occurred in the colloidal solution prior to the nucleation of sulfur particles or during ball milling. It should also be noted that the following transmission electron microscopy (TEM) analysis is biased towards stacked graphene because single graphene sheets cannot easily be observed in high-resolution cross-sectional TEM images (HRTEM).

As evidenced by TGA analysis (see Fig. S2†), a high sulfur loading of ~71.8 wt% can be achieved for this Nafion-coated FGSS composite material. Additionally, the Nafion-coated FGSS nanocomposite exhibits a XRD pattern similar to that of elemental sulfur, albeit with much lower peak intensity (Fig. 2). A small diffraction peak at $2\theta = 24.04°$ (inset in Fig. 2) corresponds to the (0002) spacing of the graphene stacks.[30] BET measurements show that the intercalation of sulfur nanoparticles between functionalized graphene sheets/stacks (FGS) reduces the surface area from 578.2 m^2/g for the pure FGS to 8.14 m^2/g for the nanocomposite material. This result is not surprising since the sulfur material has an intrinsically low surface are of 0.23 m^2/g (see Fig. S3†).

The tap density of the FGSS nanocomposite was 0.92 g/cm^3. As a comparison, the tap density of mesoporous carbon/sulfur composites with similar sulfur loading, also prepared in our laboratory, was measured to be about 0.35–0.40 g/cm^3. When pressed to pellets at 670 MPa, the pellet density of FGSS composite increased to 1.95 g/cm^3, and that of the mesoporous carbon/sulfur increased to 0.92 g/cm^3. Based on these measurements it appears that the closely

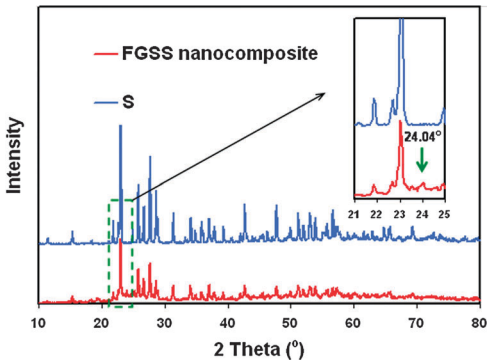

Fig. 2 XRD patterns of elemental sulfur (blue curve) and the FGSS nanocomposite (red curve). Inset shows an enlargement of the area around the (0002) diffraction peak of the stacked graphene.

stacked FGSS sandwich-type architecture has a high specific volumetric density.

In Fig. 3a, we show the cyclic voltammetry (CV) profile of a Nafion-coated FGSS nanocomposite electrode. The measurement was conducted at a scan rate of 0.1 mV s^{-1} in the voltage range of 1.0 to 3.0 V *vs.* Li/Li^+. The current response in Fig. 3a can be attributed to the intrinsic redox reaction of sulfur because the graphene stacks only function as an electron conductor in this operating potential range. During the cathodic scan, two main reduction peaks around 2.3 and 2.0 V were observed, suggesting a two-step reduction of sulfur. According to the electrochemical reduction mechanism for sulfur electrodes,[4,16] the peak around 2.3 V corresponds to the reduction of the elemental sulfur and the electrolyte to form lithium polysulfide (Li_2S_n, $4 \leq n < 8$). The peak around 2.0 V is ascribed to the decomposition of the polysulfide chain in lithium polysulfide to produce insoluble lithium sulfide (Li_2S_2 or Li_2S). It is worth noting that there is a small peak between the two main reduction peaks, suggesting the formation of low-order polysulfides (S_6^{2-} or S_4^{2-}) from S_8^{2-}.[4,16] In the subsequent anodic scan, only one intensive oxidation peak was observed at ~2.6 V. Most likely the high potential polarization between lithium polysulfide and insoluble lithium sulfide causes an overlap of the two expected reduction peaks, and only an envelope curve is observed. Little change of current or potential for the redox peaks is noticeable in subsequent scans. For uncoated FGSS nanocomposites (inset in Fig. 3a), however, there is an apparent decrease of the reduction peak over multiple scans, implying a fading discharge capacity with charge/discharge cycles. The abnormal increase in the oxidation peak current suggests the dissolution and migration of polysulfides. The absence of this decay in the Nafion-coated FGSS sample consequently indicates reduced dissolution of polysulfides.

The battery performance was tested in a coin cell using constant-current charge–discharge. Metallic Li was used as the anode. All capacity values were calculated on the basis of sulfur mass. Fig. 3b shows a typical first charge–discharge profile of a Nafion-coated FGSS nanocomposite obtained at a constant current of 168 mA g^{-1} between 1.0 and 3.0 V, which corresponds to a 0.1C rate. The discharge–charge voltage plateaus correspond very well with the peaks in the CV curve

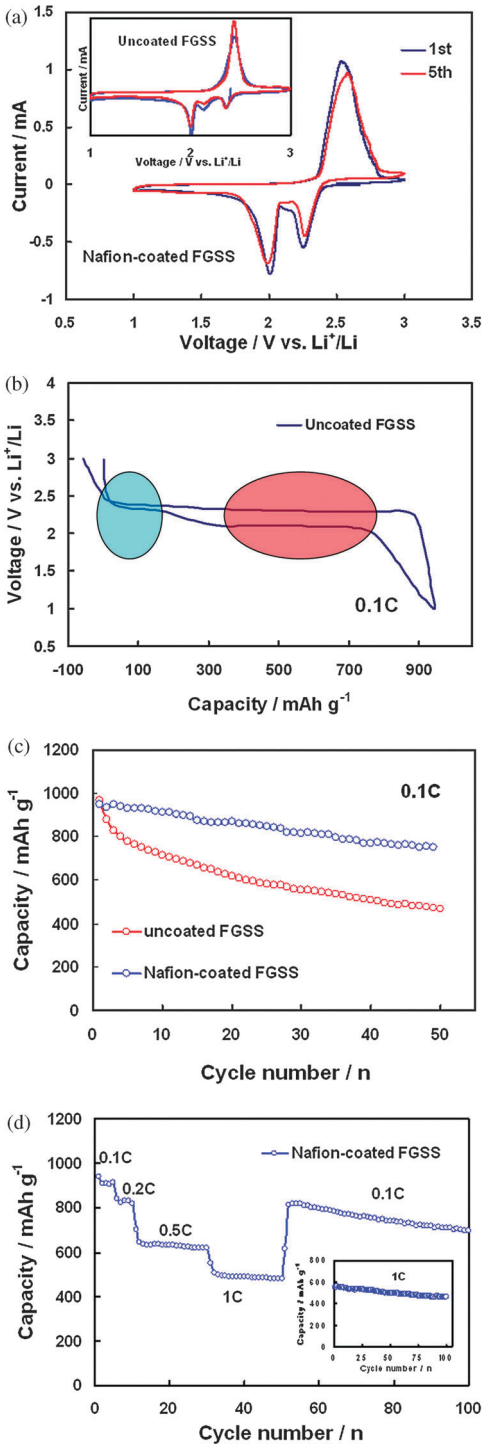

Fig. 3 Electrochemical characterization and battery performance of the FGSS nanocomposite with and without Nafion coating. (a) CV curve of the Nafion-coated FGSS nanocomposite between 1.0 and 3.0 V recorded at a potential sweep rate of 0.1 mV s^{-1}. Inset shows the CV curve of the FGSS nanocomposite without Nafion-coating. (b) Initial charge–discharge profile of the uncoated FGSS nanocomposite between 1.0 and 3.0 V at a current density of 168 mA g^{-1} (0.1C). (c) Cycle performance of the FGSS nanocomposite with and without Nafion-coating at a current density of 168 mA g^{-1} (0.1C). (d) Discharge capacity of the Nafion-coated FGSS nanocomposite as a function of charge/discharge cycles at different charge–discharge current densities of 168 (0.1C), 334 (0.2C), 840 (0.5C) and 1680 mA g^{-1} (1C), respectively. Inset shows the cycle stability of the Nafion-coated FGSS nanocomposite at a current density of ~1680 mA g^{-1} (1C).

in Fig. 3a. The two plateaus in the charge curve have a very close potential interval consistent with the fact that only one detectable anodic peak was observed in the oxidization branch of the CV curve (Fig. 3a). The wide charge–discharge potential plateau gap, corresponding to the reaction between lithium polysulfide and Li_2S (marked in red in Fig. 3b), is consistent with the peak at ~2.0 V in the CV. The charge–discharge potential plateau gap corresponding to the reaction between sulfur and lithium polysulfide (marked in blue in Fig. 3b) is narrow, consistent with the peak at ~2.3 V in the CV. The FGSS nanocomposite electrode delivered a reasonably high initial discharge capacity of 950 mAh g^{-1}. This can be converted to a volumetric capacity of ~870 mAh cm^{-3} (calculated from the whole electrode), which compares favorably with other carbon based materials. Fig. 3c shows the cycle performance of FGSS nanocomposites with and without Nafion-coating at a current density of 168 mA g^{-1} (0.1C). The uncoated FGSS electrode has ~52% retention of its initial capacity after 50 cycles. The Nafion-coated FGSS electrode, on the other hand, shows a much improved cycling performance with 79.4% capacity retention after 50 cycles at a 0.1C rate (Fig. 3c). This is in agreement with the greater stability of the redox peaks in the CV curve of Nafion-coated FGSS (Fig. 3a). The capacity retention increases significantly by ~27% compared to the uncoated electrode, while the initial discharge capacity was not significantly affected by the coating.

The Nafion coating also plays an important role in improving the cycling performance. Most importantly, the Nafion polymer exhibits an excellent chemical and electrochemical stability because of its polytetrafluoroethylene backbone. The Nafion polymer forms a dense protective film, coating the surface of graphene-sulfur nanocomposites (FGSS) and the edges of the graphene stacks and thus reduces the diffusion of polysulfide into the electrolyte from the spaces between individual graphene sheets/stacks. Secondly, Nafion polymer is a cation exchange material with a high density of negatively charged sulfonate groups. This allows the penetration of Li^+ cations into the nanocomposite electrode while at the same time suppressing polysulfide anions from diffusing across the Nafion barrier because of static-electric repulsion. Overall this leads to better cycle stability.

The battery testing data presented above indicates that the sandwich-type structures of the nanocomposite material with a higher sulfur loading compared to the mesoporous carbon nanocomposites,[9] exhibits good electrochemical performance and the Nafion coating helps to contain the soluble polysulfide within the sandwich structure of the graphene-sulfur composite thus reducing its diffusion to the lithium anode. Furthermore, excellent rate performance is observed with the nanocomposites (Fig. 3d). The Nafion-coated FGSS electrode delivers a discharge capacity of 839, 647, and 505 mAh g^{-1} at large charge–discharge currents of 336, 840, and 1680 mA g^{-1} (*i.e.* 0.2C, 0.5C and 1C), respectively. These capacities correspond to ~89, 69, and 54%, respectively, of the value obtained at a 0.1C discharge rate (see Fig. S4 in the Supporting Information†). The long-term cycling data for the Nafion-coated FGSS nanocomposite material shows ~74.3% retention of the initial capacity after a 100 cycle test under different charge–discharge rates (Fig. 3d). In addition, the electrode has a good capacity retention of about 84.3% at a charge–discharge current of 1,680 mA g^{-1} (1C) over 100 cycles (inset in Fig. 3d). The rate performance we report here shows a significant improvement comparing to a previous report by Lai *et al.*,[12] in which a sulfur/highly porous carbon (HPC) composite material has yielded a reversible capacity of only ~500 mAh g^{-1} at 400 mA g^{-1} at ~0.25C.

Scanning electron microscopy (SEM) and elemental mapping analysis were used to study the electrode structure before and after cycling (Fig. S5 in the Supporting Information†). It is challenging to see detailed microstructures since it is a mixture of electrolytes, binders and the active materials. The general particle morphology and the sulfur distribution revealed by elemental mapping through EDS (energy dispersive spectroscopy) are not significantly changed (see Fig. S5 in the Supporting Information†). This suggests that the electrode materials are stable.

We attribute the good rate capability and cycling stability of the Nafion-coated FGSS electrode to the synergetic effects of the unique sandwich-type structure, the use of conductive graphene sheets as the supporting carbon material, and the Nafion coating. The sandwich-type architecture of alternating graphene stacks and sulfur nanoparticle layers provides good contact between the active sulfur material, graphene, and the current collector. This favors fast electron transport during the redox process of sulfur, leading to low electrochemical polarization. The conductivities of pressed pellets of functionalized graphene, mesoporous carbon and their corresponding sulfur composites were measured. The conductivities of FGS, FGSS, mesoporous carbon, and mesoporous carbon–sulfur composites were 5.62 S/cm, 0.61 S/cm, 0.5 S/cm, and 0.13 S/cm, respectively. A similar benefit of adding the same functionalized graphene to TiO_2–graphene nanocomposites to improve the conductivity and capacity retention at high discharge rate was previously reported.[30] The impedance of the functionalized graphene sheet-sulfur (FGSS) composite and a control sample of mesoporous carbon–sulfur (MCS) composite were also measured after the 1st charge/discharge cycle (see Fig. S6 in the Supporting Information†). The semi-circle at high frequencies corresponds to the charge-transfer behavior and the incline line at low frequencies relates to the lithium ion diffusion in the electrode material. Compared to the MCS electrode, our FGSS composite electrode exhibits a lower charge-transfer resistance. This change could be assigned to the improved conductivity and the more favorable distribution of sulfur in our FGSS nanocomposites.

Conclusion

A functionalized graphene sheet-sulfur nanocomposite (FGSS) with sandwich-type architecture was synthesized and studied as a cathode material for lithium–sulfur batteries. The unique composite structure, the good conductivity of graphene, and the cationic exchange properties of the Nafion coating that mitigates the migration of polysulfide anions all contribute to the observed good cycling stability (84.3% capacity retention over 100 cycles at 1680 mA g^{-1}). Although this novel composite material still needs to be improved

further before it becomes suitable for practical applications, this research demonstrates a new approach to improve the performance of Li–S batteries. Better graphene dispersion, optimization of the interfacial reaction with sulfur, and better coating materials to further improve the high rate capacity and capacity retention properties are needed to build on the results presented in this study.

Acknowledgements

The authors thank Dr B. Schwenzer for helpful suggestions. This research is supported by the U.S. Department of Energy (DOE), Office of Basic Energy Sciences, Division of Materials Sciences and Engineering under Award KC020105-FWP12152. Pacific Northwest National Laboratory (PNNL) is a multiprogram national laboratory operated for DOE by Battelle under Contract DE-AC05-76RL01830.

References

1 R. D. Rauh, K. M. Abraham, G. F. Pearson, J. K. Surprenant and S. B. Brummer, *J. Electrochem. Soc.*, 1979, **126**, 523.
2 J. Shim, K. A. Striebel and E. J. Cairns, *J. Electrochem. Soc.*, 2002, **149**, A1321.
3 D. Peramunage and S. Licht, *Science*, 1993, **261**, 1029.
4 V. S. Kolosnitsyn and E. V. Karaseva, *Russ. J. Electrochem.*, 2008, **44**, 506.
5 R. D. Rauh, F. S. Shuker, J. M. Marston and S. B. Brummer, *J. Inorg. Nucl. Chem.*, 1977, **39**, 1761.
6 S.-E. Cheon, K.-S. Ko, J.-H. Cho, S.-W. Kim, E.-Y. Chin and H.-T. Kim, *J. Electrochem. Soc.*, 2003, **150**, A800.
7 J. Wang, S. Y. Chew, Z. W. Zhao, S. Ashraf, D. Wexler, J. Chen, S. H. Ng, S. L. Chou and H. K. Liu, *Carbon*, 2008, **46**, 229.
8 C. D. Liang, N. J. Dudney and J. Y. Howe, *Chem. Mater.*, 2009, **21**, 4724.
9 X. L. Ji, K. T. Lee and L. F. Nazar, *Nat. Mater.*, 2009, **8**, 500.
10 J. L. Wang, J. Yang, J. Y. Xie and N. X. Xu, *Adv. Mater.*, 2002, **14**, 963.
11 M. M. Sun, S. C. Zhang, T. Jiang, L. Zhang and J. H. Yu, *Electrochem. Commun.*, 2008, **10**, 1819.
12 C. Lai, X. P. Gao, B. Zhang, T. Y. Yan and Z. Zhou, *J. Phys. Chem. C*, 2009, **113**, 4712.
13 L. X. Yuan, H. P. Yuan, X. P. Qiu, L. Q. Chen and W. T. Zhu, *J. Power Sources*, 2009, **189**, 1141.
14 F. Wu, S. X. Wu, R. J. Chen, J. Z. Chen and S. Chen, *Electrochem. Solid-State Lett.*, 2010, **13**, A29.
15 S. E. Cheon, K. S. Ko, J. H. Cho, S. W. Kim, E. Y. Chin and H. T. Kim, *J. Electrochem. Soc.*, 2003, **150**, A796.
16 Y. J. Jung and S. Kim, *Electrochem. Commun.*, 2007, **9**, 249.
17 S. E. Cheon, J. H. Cho, K. S. Ko, C.-W. Kwon, D.-R. Chang, H.-T. Kim and S.-W. Kim, *J. Electrochem. Soc.*, 2002, **149**, A1437.
18 L. X. Yuan, J. K. Feng, X. P. Ai, Y. L. Cao, S. L. Chen and H. X. Yang, *Electrochem. Commun.*, 2006, **8**, 610.
19 D. R. Chang, S. H. Lee, S. W. Kim and H. T. Kim, *J. Power Sources*, 2002, **112**, 452.
20 B. Jin, J. U. Kim and H. B. Gu, *J. Power Sources*, 2003, **117**, 148.
21 J. H. Shin and E. J. Cairns, *J. Power Sources*, 2008, **177**, 537.
22 D. Aurbach, E. Pollak, R. Elazari, G. Salitra, C. S. Kelley and J. Affinito, *J. Electrochem. Soc.*, 2009, **156**, A694.
23 J. W. Choi, G. Cheruvally, D. S. Kim, J. H. Ahn, K. W. Kim and H. J. Ahn, *J. PowerSources*, 2008, **183**, 441.
24 J. Hasosoun and B. Scrosati, *Angew. Chem., Int. Ed.*, 2010, **49**, 2371.
25 Y. Yang, M. T. McDowell, A. Jackson, J. J. Cha, S. S. Hong and Y. Cui, *Nano Lett.*, 2010, **10**, 1486.
26 H. C. Schniepp, J. L. Li, M. J. McAllister, H. Sai, M. Herrera-Alonso, D. H. Adamson, R. K. Prud'homme, R. Car, D. A. Saville and I. A. Aksay, *J. Phys. Chem. B*, 2006, **110**, 8535.
27 M. J. McAllister, J. L. LiO, D. H. Adamson, H. C. Schniepp, A. A. Abdala, J. Liu, M. Herrera-Alonso, D. L. Milius, R. CarO, R. K. Prud'homme and I. A. Aksay, *Chem. Mater.*, 2007, **19**, 4396.
28 K. I. Bolotin, K. J. Sikes, Z. Jiang, M. Klima, G. Fudenberg, J. Hone, P. Kim and H. L. Stormer, *Solid State Commun.*, 2008, **146**, 351.
29 M. D. Stoller, S. J. Park, Y. W. Zhu, J. H. An and R. S. Ruoff, *Nano Lett.*, 2008, **8**, 3498.
30 D. H. Wang, D. W. Choi, J. Li, Z. G. Yang, Z. M. Nie, R. Kou, D. H. Hu, C. M. Wang, L. V. Saraf, J. G. Zhang, I. A. Aksay and J. Liu, *ACS Nano*, 2009, **3**, 907.
31 D. H. Wang, R. Kou, D. Choi, Z. G. Yang, Z. M. Nie, J. Li, L. V. Saraf, D. H. Hu, J. G. Zhang, G. L. Graff, J. Liu, M. A. Pope and I. A. Aksay, *ACS Nano*, 2010, **4**, 1587.
32 E. J. Yoo, J. Kim, E. Hosono, H. S. Zhou, T. Kudo and I. Honma, *Nano Lett.*, 2008, **8**, 2277.
33 S. M. Paek, E. J. Yoo and I. Honma, *Nano Lett.*, 2009, **9**, 72.
34 T. Ramanathan, A. A. Abdala, S. Stankovich, D. A. Dikin, M. Herrera-Alonso, R. D. Piner, D. H. Adamson, H. C. Schniepp, X. Chen, R. S. Ruoff, S. T. Nguyen, I. A. Aksay, R. K. Prud'Homme and L. C. Brinson, *Nat. Nanotechnol.*, 2008, **3**, 327.
35 S. Stankovich, D. A. Dikin, G. H. B. Dommett, K. M. Kohlhaas, E. J. Zimney, E. A. Stach, R. D. Piner, S. T. Nguyen and R. S. Ruoff, *Nature*, 2006, **442**, 282.
36 J.-Z. Wang, L. Lu, M. Choucair, J. A. Stride, X. Xu and H.-K. Liu, *J. Power Sources*, in press.
37 X. Wang, X. Zhou, K. Yao, J. Zhang and Z. Liu, *Carbon*, 2011, **49**, 133.

